ELSEVIER

www.elsevier.nl/locate/jorganchem

Journal of Organometallic Chemistry 592 (1999) 11–21

Journal of Organometallic Chemistry

A density functional study on the formation of stereoerrors in the stereoselective propene polymerization with zirconocene catalysts

John C.W. Lohrenz [1], M. Bühl [2], M. Weber, Walter Thiel[2] *

Organisch-Chemisches Institut der Universität Zürich, Winterthurerstrasse 190, CH-8057 Zurich, Switzerland

Received 25 May 1999; accepted 27 July 1999

Abstract

Recent labeling experiments have detected stereoerrors in the isotactic polymerization of propene with zirconocenium catalysts, which are characterized by a deuterium transfer from the polymer chain to a methyl group. Using Cp_2Zr-*iso*-butyl$^+$ as a model system, two alternative mechanisms leading to the observed products are investigated using fully nonlocal levels of density functional theory (DFT). The direct hydrogen transfer starting from a γ-agostic intermediate requires an overall activation relative to the β-agostic resting state in excess of 200 kJ mol^{-1} and can be excluded. The sequential mechanism involves a (i) β-elimination to yield an initial *iso*-butene π-complex; (ii) a subsequent internal rotation of this π-complex; and (iii) reinsertion of the olefin into the Zr–H bond via two consecutive formations of β-agostic interactions, with maximum relative energies along this path between 35 and 54 kJ mol^{-1} (depending on functionals and basis sets employed). The subsequent steps are the reverse of the first three steps and can lead to an inverted *iso*-butyl complex with migrated deuterium. Although certain barrier heights are somewhat sensitive to the density functional employed (BP86 vs. B3LYP), the sequential mechanism is much more favorable energetically. Loss of olefin from the intermediate π-complex is endothermic by 104–114 kJ mol^{-1} and should therefore not occur.

Keywords: DFT; Stereoerrors; Propene polymerization; Zirconocene catalysts

1. Introduction

The amazing stereoselectivity of zirconocene catalysts in the polymerization of propene to isotactic and syndiotactic polypropene [1] has led to their incorporation in industrial processes. After the first observation of an isotactic polymerization of propene by Kaminsky et al. [2], much effort was spent in order to increase the stereoselectivity of the catalysts. Over the years much insight into the underlying stereoregulating mechanisms was gained both from experiment [1,3,4] and more recently from calculations [5–8]. It is the current belief that the orientation of the inserting olefin is controlled by the last inserted monomer, which itself is oriented in a way to minimize steric interactions with the (bulky) ligands, implying that systematic substitutions at the ligands can induce a favorable orientation of the polymer chain. Thus, optimization of the catalysts has so far usually been directed towards an increased stereodifferentiation between the two possible orientations of the inserting olefin (Scheme 1).

According to Scheme 1, insertions with the wrong orientation of the olefin will lead to stereoerrors in the polymer chain. Recent labeling experiments, however, point to an additional cause for stereoirregularities. Leclerc and Brintzinger [9,10] investigated the polymerization of *cis*- and *trans*-propene-d_1 by $Et(Ind_2)ZrCl_2$/MAO in order to shed light on the importance of agostic interactions in the transition state of the insertion (Scheme 2).

NMR analysis of the resulting polymers gave some surprising results. As expected, the polymer consisted to a high degree of (isotactic) mmmm pentades and deuterium incorporation exclusively in the polymer chain.

* Corresponding author. Tel.: +49-208-306-2150; fax: +49-208-306-2996.

E-mail address: thiel@oci.unizh.ch (W. Thiel)

[1] Present address. Bayer AG, ZF-MFK Material- und Synthesemodelling, Geb. Q18, D-51368 Leverkusen, Germany.

[2] Present address. Max-Planck-Institut für Kohlenforschung, Kaiser-Wilhelm-Platz 1, D-45470 Mülheim, Germany.

0022-328X/99/$ - see front matter
PII: S0022-328X(99)00438-6

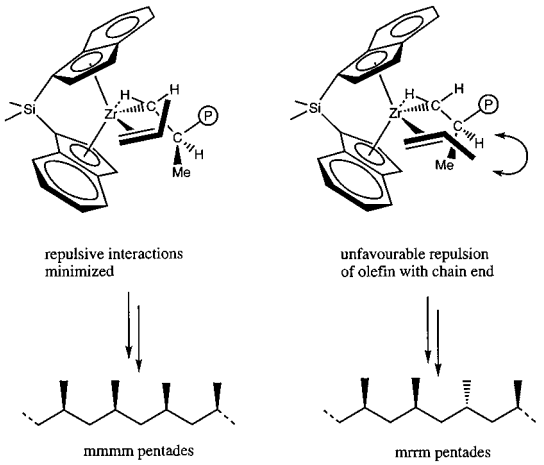

Scheme 1. Stereodifferentiation of the inserting olefin as induced by the orientation of the last-inserted monomer.

Furthermore, the normal amount of mrrm pentades, which indicate a stereoerror due to one inverted stereocenter, could be found. Interestingly, the corresponding methyl group was characterized by a ^{13}C-NMR resonance which coupled to a deuterium atom, whereas regular insertion should lead to deuterium in the backbone only. It was found that about 80% of the inverted methyl groups contained deuterium. Obviously, after insertion a rearrangement must have taken place, which at the same time led to inversion of the stereocenter. The mechanism of this rearrangement will be studied in this article by density functional theory (DFT). Salient features of this mechanism have recently been addressed by DFT calculations [11]. We now present a more comprehensive theoretical study of this process calling special attention to the sensitivity of the results to the density functionals employed.

The reliability of DFT calculations for such applications was proven by a series of investigations [12–22] on the insertion and propagation mechanism in the polymerization of ethylene with several metallocenes, ansa-metallocenes as well as mono-Cp-catalysts like the constraint-geometry catalyst [19]. Furthermore, the underlying mechanism of chain termination was studied in detail, and the calculated molecular weights of the polymers were in good agreement with experimentally determined values [17]. Finally, good agreement between correlated ab initio and DFT calculations has also been found for related systems [23].

In most studies of these quite sizeable complexes, geometries had been optimized with the more economic local density approximation, followed by energy evaluations employing the more accurate, but also more expensive non-local (gradient-corrected) functionals. If local and non-local potential-energy surfaces would differ significantly, such a procedure would introduce nonsystematic errors in the theoretical results. We now present a study involving refinement and characterization of all stationary points on a non-local level of DFT and an assessment of different functionals and basis sets, which turn out to affect specific aspects of the reaction path, but not its general viability.

2. Computational details

Initial studies employed the program system ADF1.1.3 and ADF2.0.1, developed by Baerends et al. [24–28] and the following STO (Slater-type orbital) basis set: zirconium (4s, 4p, 4d, 5s, and 5p): uncontracted triple-ζ [29,30]; carbon (2s, 2p) and hydrogen (1s): double-ζ [29,30], augmented with a single 3d or 2p polarization function, respectively. No polarization functions were employed for carbon and hydrogen atoms of the Cp rings. The cores ($1s^2 2s^2 2p^6 3s^2 3p^6 3d^{10}$ on Zr; $1s^2$ on C) were treated by the frozen core approximation [31]. In order to fit the molecular density and to represent Coulomb and exchange potentials accurately, a set of auxiliary s, p, d, f, and g STO

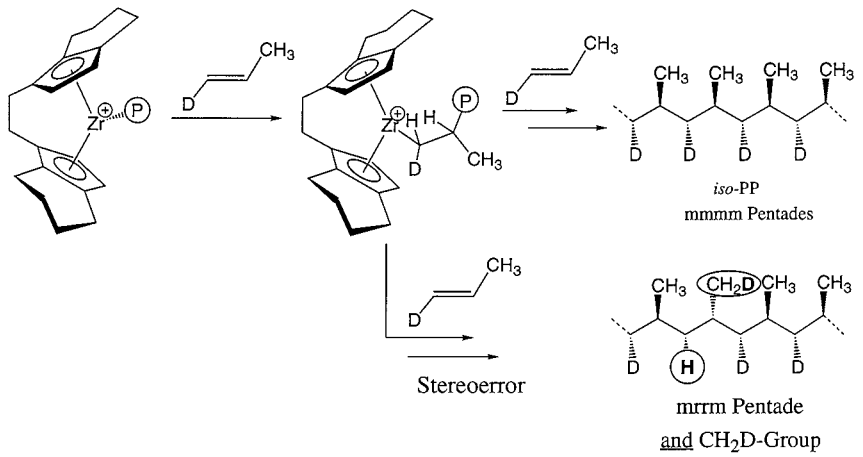

Scheme 2. Isotactic polymerization of *trans*-(*cis*-)propene-d_1 with $Et(Ind_2)ZrCl_2$/MAO and formation of stereoerrors [9].

functions [32] centered on all nuclei was used in every SCF cycle. Geometry optimizations were carried out at the level of the local density approximation (LDA [33]). Energy differences were determined from single-point gradient-corrected DFT calculations using Becke's nonlocal exchange functional [34] and Perdew's nonlocal correlation functional [35]. This level is denoted BP86//LDA.

Geometries were then fully optimized employing the BP86 functional combination as implemented in the Gaussian 94 program [36], together with a fine integration grid (75 radial shells with 302 angular points per shell, no fitting of Coulomb and exchange potentials) and the following, contracted GTO (Gaussian-type orbitals) basis set (denoted AE1): Zr: (17s 11p 8d) [37] augmented with two diffuse p and one diffuse d functions [38] and contracted to [633311/53311/5211]; C and H: 6-31G* [39,40] (no polarization functions on the Cp rings); this level is denoted BP86/AE1. The nature of each stationary point has been verified by harmonic frequency calculations at that level. Effects of larger basis sets have been probed by single-point energy calculations employing the BP86/AE1 geometries and the following contracted basis set (denoted ECP2): Zr: relativistic ME-fit effective core potential (ecp) together with the corresponding valence basis in the contraction [311111/21111/411] [41]; C and H: Dunning's polarized triple-ζ basis [42] (contraction [62111/411/1] and [311/1], exponents of polarization functions 0.8), without polarization functions on the Cp rings. Single-point energy calculations have been performed at the BP86/ECP2 and B3LYP/ECP2 levels, the latter employing Becke's three-parameter hybrid functional [43], together with the correlation functional of Lee, Yang, and Parr [44].

If not otherwise stated, all energies given in the text and Figures refer to the BP86/AE1 level of theory.

The present study is based on the generally accepted assumption that an unsolvated metallocene cation acts as the active catalytic center. Interactions with the counterion or the solvent are neglected [45]. Work on the role of the counterion is in progress and will be published elsewhere [46].

3. Mechanisms for stereoerror formation

As mentioned in Section 1, there are two possible mechanisms that can explain the isomerization shown in Scheme 2. The first one is a direct transfer of a hydrogen atom from the γ-methyl group to the α-carbon, with simultaneous Zr–C_γ bond formation and Zr–C_α bond cleavage (Scheme 3; path A). It may be expected that a strong agostic interaction or even temporary formation of a Zr–H bond will greatly reduce the barrier for the C–H bond cleavage. A similar *intermolecular* mechanism was calculated for the chain-terminating H-exchange between the chain end and an

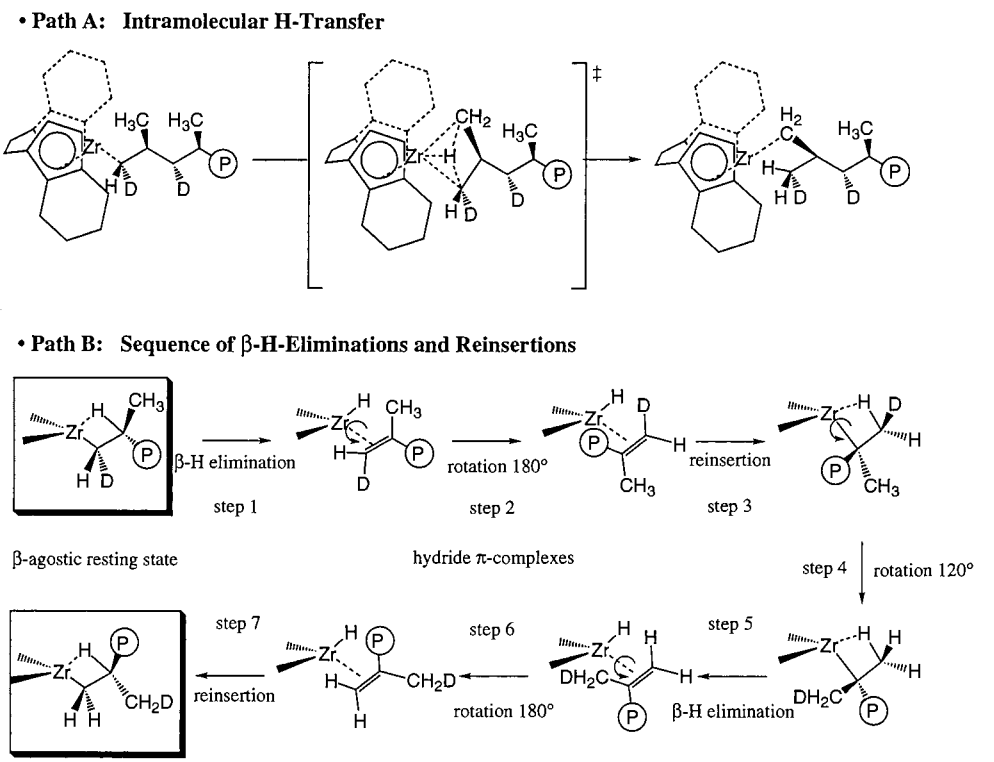

Scheme 3. Mechanisms for the formation of stereoerrors.

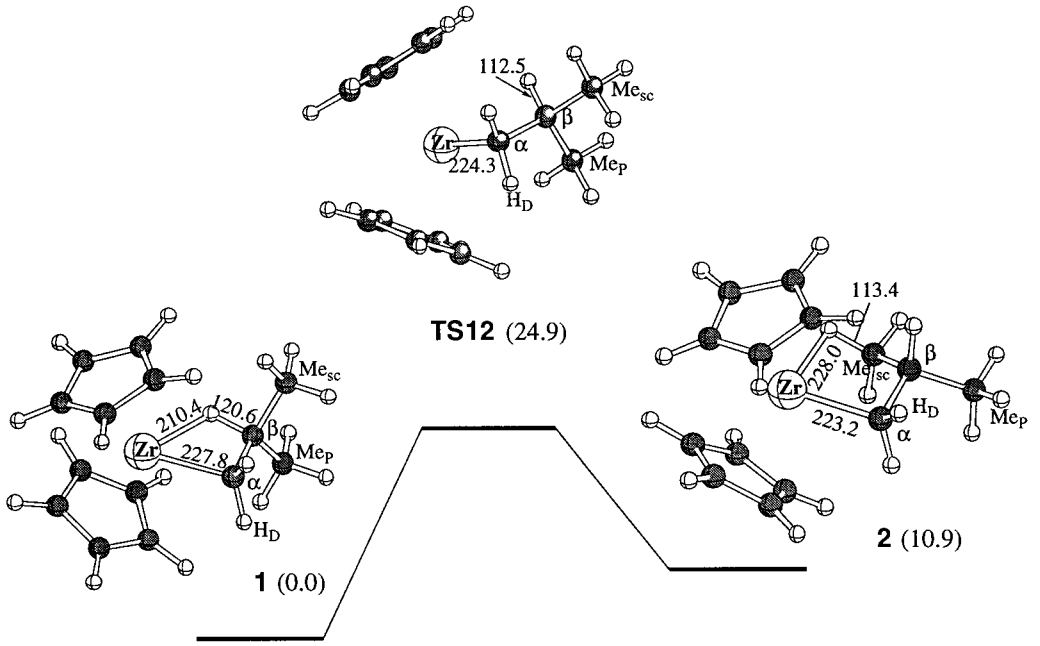

Fig. 1. Structure of the β-agostic resting state **1** between two insertions, the isomeric γ-agostic complex **2** and the transition state **TS12** between both; relative energies in [kJ mol^{-1}], bond lengths in [pm].

olefin [17]. The intramolecular H-transfer should, however, suffer from strain energy due to the presence of a small ring in the transition state. Busico and co-workers proposed an alternative path, a complex sequence of β-eliminations, reorientations, and reinsertions that would lead to the same product (Scheme 3; path B) [47–49]. A similar mechanism was earlier suggested to account for the rearrangement of 2,1-regioinverted units to 1,3-units, which competes with olefin insertion into the secondary Zr–alkyl bond [50,51]. In path B, the initial β-elimination is expected to be the rate-determining step, since earlier theoretical investigations came to the conclusion that β-eliminations are very unlikely for chain termination reactions because of a high reaction enthalpy [12]. After the β-elimination, rotation of the olefin has to take place in step 2, followed by reinsertion into the Zr–H bond (step 3). This converts the α-methylene unit bearing the deuterium atom into a terminal methyl group. In step 4 the chain end has to reorient before another β-elimination (step 5) can take place, this time eliminating hydrogen from the second methyl group. Step 6 resembles step 2 and consists of a reorientation of the olefin. Reinsertion into the Zr–H bond (step 7) finally leads to an inverted β-carbon center and migration of the deuterium atom into the methyl group.

Prosenc and Brintzinger have recently presented DFT calculations in support of this stepwise mechanism [11]. We will refine the potential-energy surface at a higher, non-local DFT level, first turning to the structure of the resting state of the active catalyst, followed by detailed discussions of paths A and B. Finally, an assessment of effects of functional and basis set on the key barriers is presented.

4. The structure of the ground-state model

As a model for the growing polymer chain we chose an *iso*-butyl group. This group is needed to describe correctly the orientation around the metal center after insertion of a propene into the chain end. One of the two methyl groups represents the polymer chain and will be designated as Me_P, whereas the second methyl group Me_{sc} stems from the last inserted propene. Introducing a formal distinction between the two methyl groups, the β-carbon atom becomes chiral (r in Fig. 1 assuming Me_P to be heavier than Me_{sc}). To facilitate comparisons with the experimental results [9,10], we will mark the *trans*-hydrogen at the α-carbon atom as H_D to denote a deuterium atom in that position.

In Fig. 1, two possible orientations of the chain end are shown. Complex **1** corresponds to the resting state with the agostic bond to the tertiary carbon atom in β position. Rotation about the Zr–C(α) bond via **TS12** affords **2**, where the agostic bond involves a hydrogen atom of the side-chain methyl group in γ position. The agostic interaction is stronger in **1** than in **2**, as evidenced by a longer C–H bond (121 vs. 113 pm) and a shorter Zr–H distance (210 vs. 228 pm). Consequently, **1** is more stable than **2**, by 11 kJ mol^{-1}, in spite of some steric hindrance between the methyl groups and the Cp ligands in **1**. The barrier between **1** and **2** is low, 25 kJ mol^{-1} at BP86/AE1, suggesting facile intercon-

version between the two isomers. At the BP86//LDA level, the energetic separation between **1** and **2** is much larger, 54 kJ mol^{-1}.

Qualitatively, the results for the *iso*-butyl complexes **1** and **2** are similar to those for the *n*-butyl complexes [17] where the β-agostic structure is also more stable than the γ-agostic one due to a stronger agostic interaction (judging from the LDA bond lengths). Quantitatively, the BP86//LDA energy difference is smaller in the *n*-butyl complex (27 kJ mol^{-1} [17]) than in the *iso*-butyl complex (54 kJ mol^{-1}), indicating a differential stabilization of the β-agostic structure **1** through the presence of an additional methyl group at C_β.

5. Direct H-transfer

Direct H-transfer from the methyl group in the γ-position will most likely occur out of an orientation like that in **2**. A transition structure for this process has been located imposing C_s symmetry (**TS22**, see Fig. 2); for our model system the resulting **2′** is the mirror image of **2**. The Zr–H_1 distance in **TS22** (191.1 pm) is only slightly longer than a normal Zr–H bond (see below). The computed bond order, however (from natural population analysis [52] using Wiberg's definition [53]) is only 0.14. Likewise, reduced bond orders are obtained between Zr and C_α (0.47) and between C_α and H_1 (0.38), indicative of a four-center-four-electron bond. Key geometrical parameters of **TS22** are in line with those of the previously investigated transition state for intermolecular H-transfer in a possible chain termination [17].

Inspection of the labels in **2** and **2′** confirms that the desired rearrangement has taken place: the configuration at C_β is reversed and a deuterated methyl side chain is formed (Fig. 2).

The intramolecular transfer enforces a four-membered ring and hence leads to a small C_α–C_β–C_γ angle of only 95.98. The associate strain contributes to the high activation barrier of 204 kJ/mol relative to the γ-agostic complex **2** and 215 kJ mol^{-1} relative to the β-agostic resting state **1** (BP86//LDA level: 244 kJ mol^{-1}). All other zirconocene reactions studied so far (insertion and chain termination, as well as an alternative insertion path from the back side) have much smaller barriers [12,16]. Therefore we conclude that direct H-transfer is not a feasible path.

In addition to the imaginary mode for H-transfer ($v = 1443i$ cm^{-1}), a second imaginary frequency ($22i$ cm^{-1}) is computed for **TS22**, corresponding to a rotation of the two Cp rings with respect to each other; the actual transition state may thus have C_1 symmetry, but a very similar energy.

6. The sequential isomerization

6.1. β-Hydride elimination

The tentative sequence shown in Scheme 3 can be split up into seven elementary steps, three of which occur twice in our model system: step 7 corresponds to

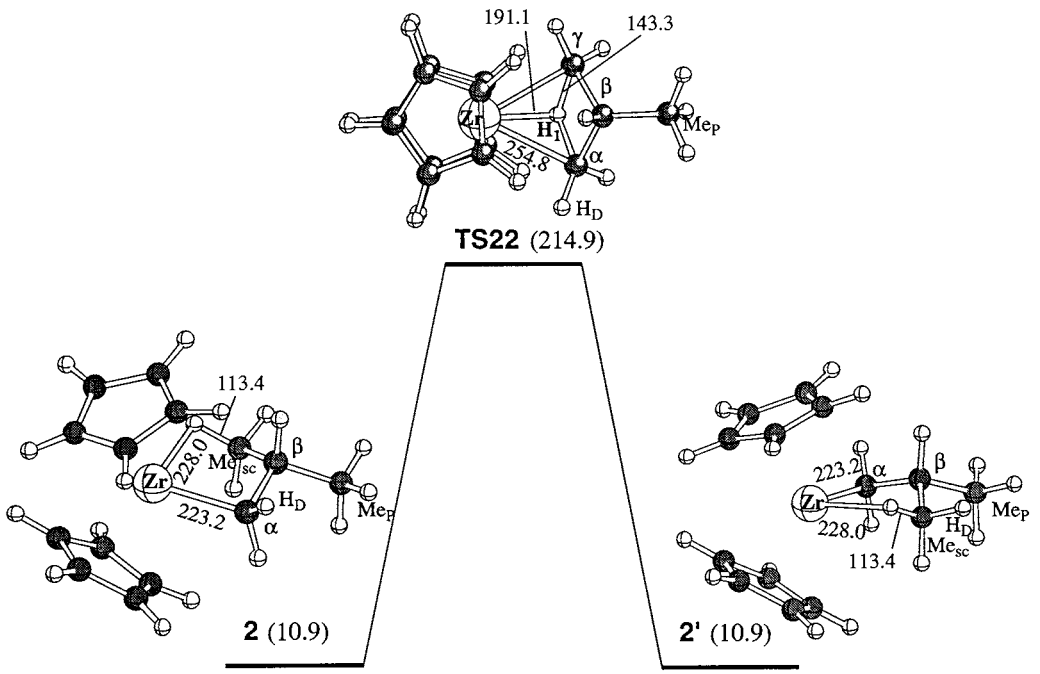

Fig. 2. Reaction path for the direct intramolecular H-transfer; relative energies in [kJ mol^{-1}], bond lengths in [pm].

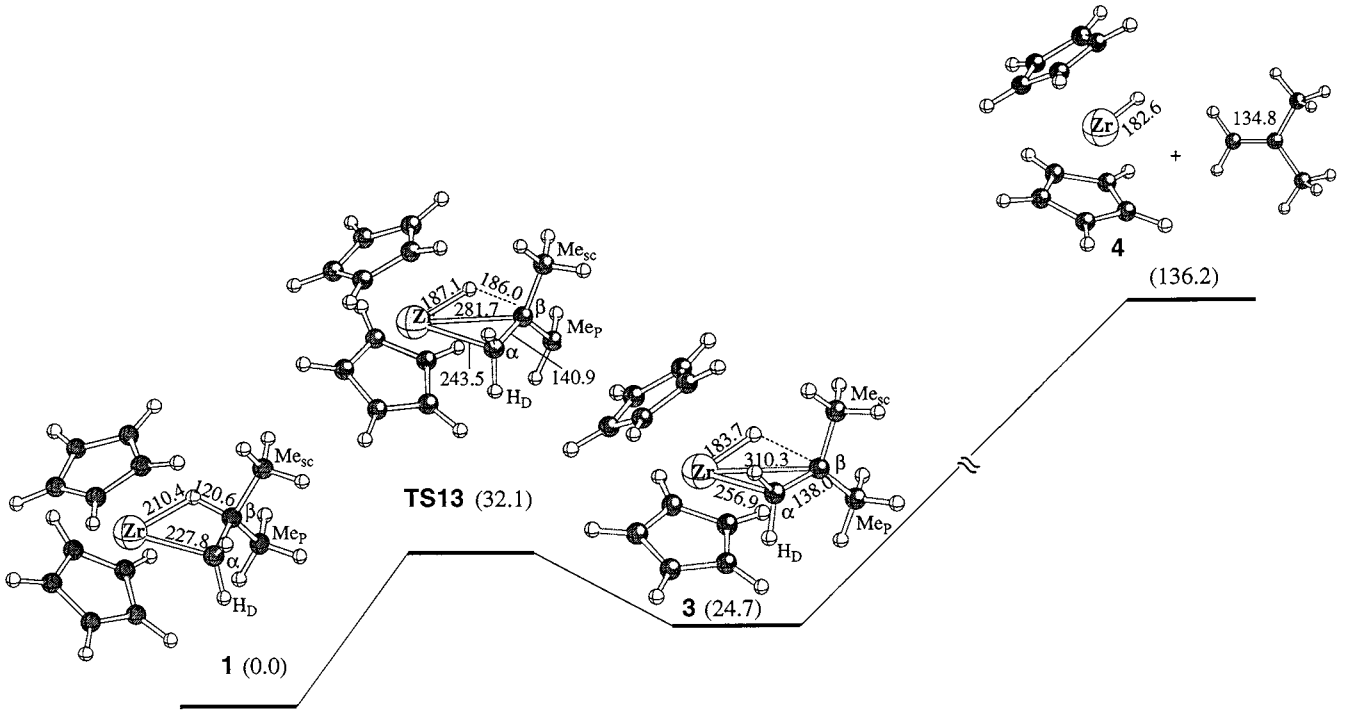

Fig. 3. Formation of the initial π-complex **3**; relative energies in [kJ mol^{-1}], bond lengths in [pm].

the back reaction of step 1; the same holds for steps 6 and 2 as well as 5 and 3. In the following we shall discuss each distinct step separately. The sequence starts with a β-hydrogen elimination from the β-agostic resting state **1**, affording the hydride π-complex **3** (see Fig. 3) which lies 24.7 kJ mol^{-1} above **1**. The activation barrier via **TS13**, 32.1 kJ mol^{-1}, is comparable to that for the intermolecular H-transfer [17]. Dissociation of **3** to yield the olefin and the zirconocene–hydride cation **4** requires 111.5 kJ mol^{-1} (136.2 kJ mol^{-1} with respect to **1**) which makes chain termination via β-elimination unlikely.

The hydride π-complex **3** shows no symmetry and contains a short Zr–H bond (183.7 pm). The short C–C distance of 138.0 pm indicates a double bond in the olefin, in accordance with the corresponding Wiberg bond index of 1.67 (cf. 1.91 in free isobutene). The olefin in **3** is unsymmetrically bound with a short (C_α–Zr: 256.9 pm) and a long (C_β–Zr: 310.3 pm) distance. This is probably at least partly due to the steric bulk around C_β carrying two methyl groups that may interfere with the Cp ligands. In the LDA geometries hitherto employed, this asymmetric bonding in the olefin is somewhat less pronounced, cf. 255 versus 301 pm [11] or 253 versus 288 pm (BP86//LDA, this work).

6.2. Rotation of iso-butene in *3*

The next step in the proposed reaction sequence corresponds to a 180° rotation around the Zr–olefin axis. The computed rotation profile, characterized by the key minima and transition states, is depicted in Fig. 4.

In addition to **3**, two other rotamers have been located after rotations of approximately 90° (**5**) and 180° (**6**). The perpendicular form **5** is the most stable of these, and complete rotation appears to be largely unhindered with computed barriers no larger than 6.5 kJ mol^{-1} relative to **5** (via **TS56**, 29.1 kJ mol^{-1} above **1**). Rotamer **5** is characterized by an even larger asymmetry in the binding of the olefin (the latter is identified by the short C_α–C_β distance of 137.5 pm and by the Wiberg bond index of 1.69), with Zr–C distances of 253.2 and 326.7 pm. Apparently, steric repulsion between the methyl and the Cp groups is somewhat less pronounced in **5** than in **3** (cf. the smallest nonbonded H···H distances of 242 and 230 pm, respectively).

6.3. Reinsertion of iso-butene into the Zr–H bond

Reinsertion of the olefin into the Zr–H bond in **6** would lead to $Cp_2Zr(t\text{-Bu})^+$, for which two strong β-agostic interactions have been found [11] (cf. **8** in Fig. 5).

No direct transition state between **6** and **8** could be located on the BP86/AE1 potential-energy surface. Rather, an additional intermediate occurs (**7**) which is characterized by a single γ-agostic interaction. Intermediate **7** is not connected to the *trans*-rotamer **6**, but to the perpendicular form **5**, via **TS57** (Fig. 5). This has

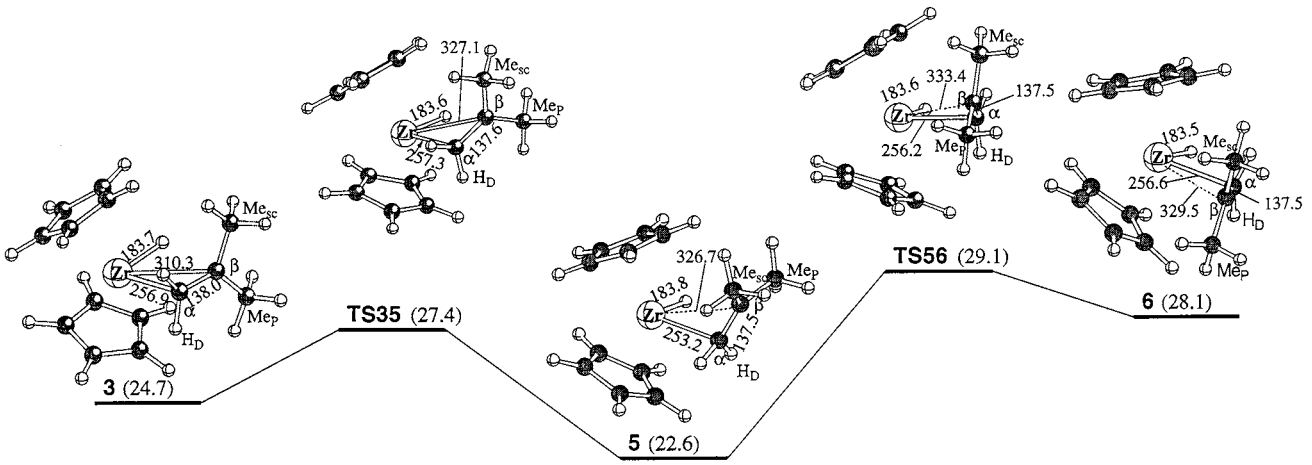

Fig. 4. Rotational profile of π-complex **3**; relative energies in [kJ mol^{-1}], bond lengths in [pm]; the H–Zr–C_α–C_β dihedral angle changes from −1.2° (**3**) via 37.4° (**TS35**), 83.0° (**5**), and 152.1° (**TS56**) to 180.0° (**7**).

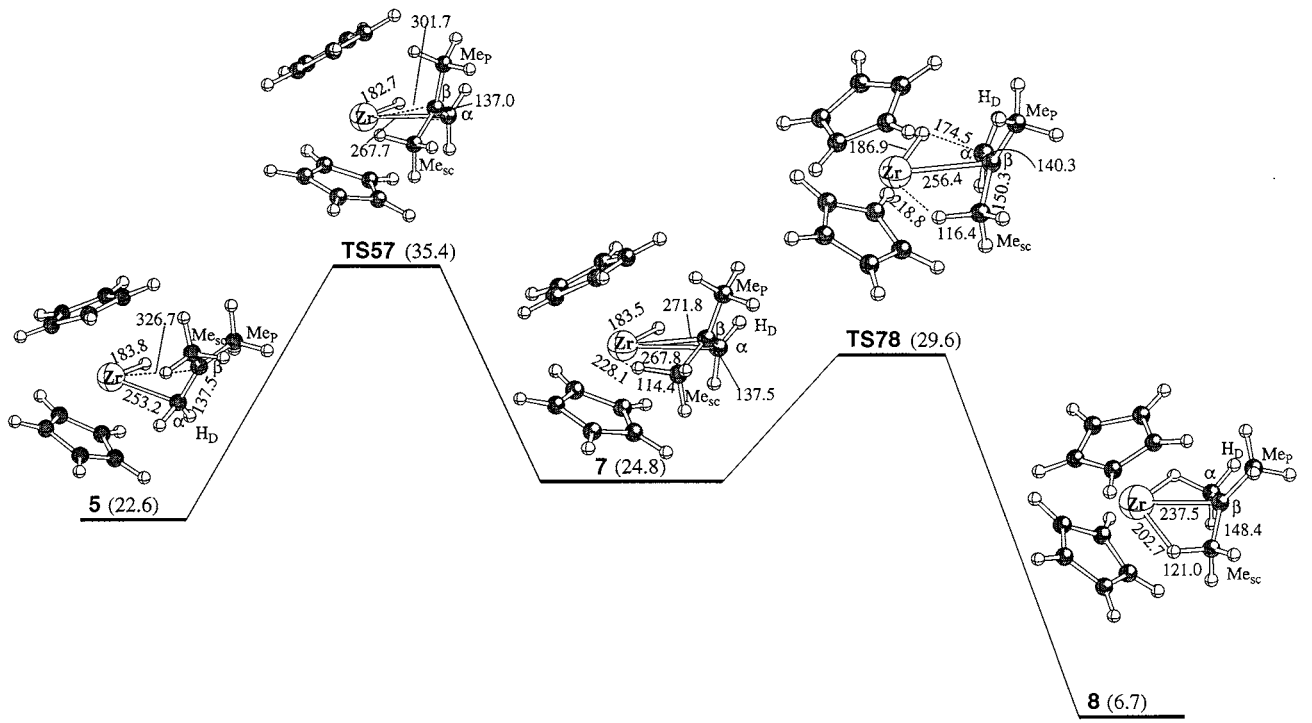

Fig. 5. Reinsertion of *iso*-butene into the Zr–H bond; relative energies in [kJ mol^{-1}], bond lengths in [pm].

been verified by following the relevant parts of the intrinsic reaction coordinate [54,55]. Formation of the first agostic interaction (via **TS57**) is slightly higher activated (35.4 kJ mol^{-1}) than formation of the second (via **TS78**, 29.6 kJ mol^{-1}). Compared to the Zr–C bond in **1**, that in **8** (involving a tertiary carbon atom) is significantly weakened, cf. the elongation from 227.8 to 237.5 pm and the reduction of the bond index from 0.72 to 0.62 in going from **1** to **8**. Nevertheless, **8** is only 6.7 kJ mol^{-1} above **1**, apparently due to the stabilizing effect of the two agostic interactions.

Complex **8** is nearly symmetric with respect to the X–Zr–X plane (X: center of Cp ring). Upon reversal of the reaction sequence, i.e. from **8** to **1**, the stereorerror in question is produced when the agostic interaction between Zr and the hydrogen atom of the Me_{SC} hydrogen is cleaved before the one between Zr and the hydrogen atom at C_α, which had been formed last. For our model system, the subsequent minima and transition structures are the respective mirror images of the structures displayed in Figs. 3–5, eventually producing **1′** with the stereoerror.

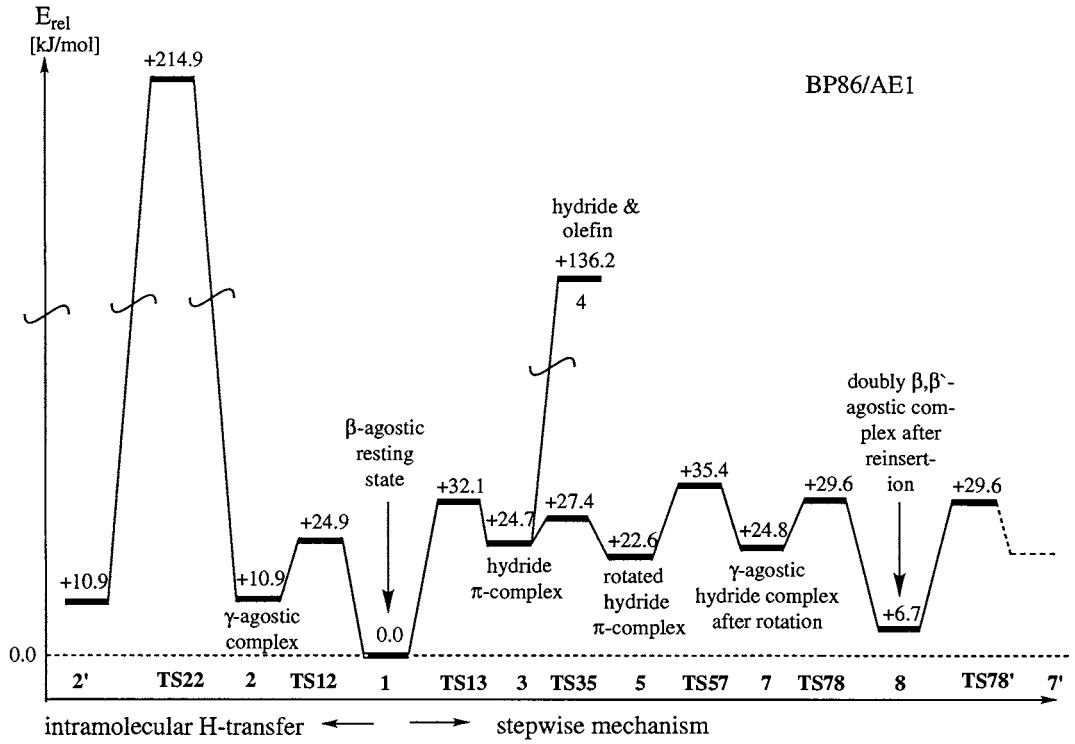

Fig. 6. Comparison of direct H-transfer and the sequential mechanism; all energies in [kJ mol^{-1}] relative to the β-agostic resting state **1**.

Besides such a reversal of the multi-step process, **8** could in principle be susceptible to insertion of propene. This reaction would lead to quaternary carbon centers in the polymer backbone, which are known to occur much more rarely than stereoerrors. Propagation after insertion into secondary Zr–C bonds (i.e. after 2,1-mis-insertions) is already about 100 times slower than after insertion into primary Zr–C bonds (i.e. after the usual 1,2-insertions) [56]. Therefore, insertions into the tertiary Zr–C bond of **4** yielding quaternary carbon atoms should be even less favorable, so that the system will rather reorient and undergo β-elimination.

Fig. 6 summarizes the reaction sequence and compares it to the direct isomerization.

Despite its complexity, the sequential mechanism is energetically feasible and by far more likely than the alternative direct H-transfer. The latter is highly unfavorable, with an overall barrier of 215 kJ mol^{-1}. The highest point on the sequential pathway, on the other hand, is the formation of the first β-agostic interaction in the rotated hydride π-complex via **TS57**, which lies only 35.4 kJ mol^{-1} above the resting state **1**. At the BP86//LDA level, formation of **3** is computed to be rate-determining, but with a similar energy of activation, 41.4 kJ mol^{-1} (virtually identical to the value from Ref. [11] at a comparable level). Both values are only slightly higher than that for chain termination reactions studied earlier [17]: intermolecular H-transfer to an olefin was found to have an activation barrier of 29 kJ mol^{-1}, and an alternative vinylic C–H activation needed 30.1 kJ mol^{-1}. This clearly shows that the rearrangement from **1** to **3** and the subsequent steps are possible. Side reactions like chain termination through loss of olefin from **3** or insertion of olefin into the β-agostic intermediate **8** are less favorable.

7. Effect of basis set and exchange-correlation functionals

So far, energies on the BP86/AE1 potential-energy surface have been discussed. Table 1 summarizes relative energies upon inclusion of zero-point corrections ($\Delta E + \mathrm{ZPE}$), thermal (ΔH) and entropic corrections (ΔG) at room temperature, computed from the BP86/AE1 harmonic vibrational frequencies. Zero-point corrections generally stabilize transition states, and further thermal corrections on going to the enthalpies are very small. Entropic contributions make olefin dissociation significantly less unfavorable (cf. ΔG vs. ΔH for **4** + *i*-butene in Table 1) and tend to stabilize the π-complexes **3**, **5**, and **6** due to the softer vibrational modes in the latter. Since all vibrations have been treated as such in the statistical thermodynamic analysis, however, the computed entropies are probably not very accurate and should only be used as a rough guide. All conclusions regarding the viability of the sequential pathway and the refutation of direct H-transfer are unaffected by these thermodynamic considerations. The only qualita-

Table 1
Effect of thermodynamic corrections, basis set, and exchange-correlation functional on relative energies of stationary points [energies in kJ mol^{-1} relative to **1**]

Species	BP86//LDA	BP86/AE1				BP86/ECP2	B3LYP/ECP2
	ΔE_{rel} [a]	ΔE_{rel}	ΔE+ZPE	ΔH (298)	ΔG (298)	ΔE_{rel}	ΔE_{rel}
1	0.0	0.0	0.0	0.0	0.0	0.0	0.0
TS12		24.9	27.6	25.7	31.9	32.1	35.6
2	54.2	10.9	13.8	13.6	13.8	14.6	19.5
TS22	244.5	214.9	204.7	202.0	207.7	207.2	233.9
TS13		32.1	22.4	21.8	24.0	33.0	36.8
3	41.4	24.7	15.3	17.7	8.2	24.9	18.7
4+*i*-butene	158.1	136.2	123.0	123.8	70.0	126.2	116.2
TS35		27.4	17.8	17.8	16.6	27.6	20.7
5	29.8	22.6	13.0	15.2	6.4	23.0	17.1
TS56		29.1	19.3	19.5	17.7	29.6	23.0
6	37.1	28.1	18.9	21.0	13.2	28.6	21.5
TS57		35.4	26.3	26.2	25.8	37.9	34.3
7	17.8 [b]	24.8	18.0	17.9	20.6	28.6	37.6
TS78		29.6	21.4	19.4	26.5	33.1	53.6
8	−8.1	6.7	5.7	4.4	8.7	12.6	33.8

[a] Missing entries: transition structures have not been determined at the LDA level.
[b] Not a stationary point at the BP86//LDA level.

tive change for the stepwise mechanism is that reinsertion via **TS78** and formation of the β-agostic hydride complex via **TS57** have nearly identical free energies of activation.

How are the details of the potential-energy surface under scrutiny affected when larger basis sets and other exchange-correlation functionals are employed? This question has been addressed by single-point energy calculations using the BP86/AE1 geometries. Extension of the basis and use of a relativistically adjusted pseudopotential on Zr (BP86/ECP2 level) affords only minor changes with respect to the BP86/AE1 data (compare second and last but one column in Table 1).

Besides pure density functionals such as BP86, hybrid functionals such as the popular B3LYP combination have been successfully applied to problems in transition-metal chemistry [57]. For thermochemical data of molecules comprising first- and second-row atoms, this functional (due to its specific parametrization) usually outperforms most other ones. While a general superiority of B3LYP is less evident for transition-metal compounds, it may be instructive to see how strongly the salient features of the reaction mechanism can depend on the theoretical level. In fact, when comparing BP86/ECP2 and B3LYP/ECP2 data in Table 1, noticeable changes in the relative energies are found, in particular for the reinsertion step: **TS78** and **8** are significantly destabilized with the hybrid functional (by ca. 20 kJ mol^{-1}), and **TS78** becomes the highest point in the multi-step sequence. In addition, **7** is destabilized by such an extent (9 kJ mol^{-1}) that it is higher in energy than the transition structure for its formation, **TS57**. It is thus possible that **7** is not a minimum and that reinsertion of the olefin in **5** occurs in a single step.

8. Discussion

In the present paper we have investigated the formation of stereoerrors in the stereoselective polymerization of propene with homogeneous zirconocenium catalysts. Two pathways were studied: the direct H-transfer and a stepwise mechanism. The first pathway has a total barrier of more than 200 kJ mol^{-1}, which is higher than any other barrier calculated as yet for any elementary reaction in the homogeneous Ziegler–Natta polymerization. Propagation and chain termination have considerably lower barriers. Ring strain probably contributes to this unusually high barrier. In the transition state, the polymer chain and the metal atom form a metallacyclobutane which is bridged by a hydrogen atom.

The stepwise mechanism [11,47–49], on the other hand, involves no high-energy intermediates or excessively high barriers. Quantitative details depend somewhat on the density-functional methodology employed, but the first step, β-elimination affording the transient hydride π-complex **3**, is noticeably activated at all levels (between ca. 32 and 41 kJ mol^{-1}; this is the rate-determining step at BP86//LDA, see also reference [11]). Loss of olefin from this π-complex is endothermic between ca. +116 and +136 kJ mol^{-1} and is thus not very likely. This process would lead to chain termination while the zirconocenium hydride could start a new polymer chain. Rotation of the olefin in the π-complex is largely unhindered and will be followed by reinsertion of the olefin, leading to **8** with a quaternary carbon atom bound to the metal center. This reinsertion is indicated to proceed via an intermediate γ-agostic π-

complex **7** (possibly also in a single step, as suggested by the B3LYP data) and involves the highest total barrier in the sequence found in this study (ca. 35–54 kJ mol^{-1} relative to **1**). It is probably safe to assume that insertion into tertiary Zr–C bonds such as in **8** is highly unfavorable (see [56]) and chain propagation at this stage becomes unlikely. Insertion of an additional propene monomer would lead to quaternary carbon centers in the backbone, which is not observed experimentally. Thus, from this point only two reactions can take place: (i) β-elimination back to the hydride complex, either under retention or inversion; and (ii) β-hydride transfer to another olefin leading to chain termination. Since the β-H-transfer reaction to ethylene was calculated to have a barrier of 28.2 kJ mol^{-1} (BP86//LDA level) [17], and since in **8** most of the space needed for olefin complexation is taken up by the two agostic interactions, β-H-elimination seems more likely. The remaining steps are the reverse of those leading to **8**, affording eventually **1** under retention or inversion of the β-carbon, depending on which of the two β-agostic interactions in **8** is broken first.

These considerations corroborate earlier DFT results [11] and suggest that stereoerrors will be formed by a complex sequence of β-eliminations, rotations, and reinsertions. Interestingly the same mechanism holds for the formation of 1,3 inserted units in the polymer chain after 2,1 regioirregular insertions of propene. In this case only steps 5–7 (β-elimination from the α-methyl group, rotation of the olefin, and reinsertion into the Zr–H bond) are necessary. The fact that less-active catalysts exclusively form 1,3 units, while the more active catalysts like $Me_2Si(ind)_2ZrCl_2$/MAO lead to a higher degree of head, head errors (i.e. normal insertion after a 2,1 regioerror) is in line with our conclusions. Insertion into the less active complexes is slow while β-elimination can take place more readily, so that more inversions at the chain can be observed.

We have already pointed out that insertion into the tertiary Zr–C bond is unlikely and β-hydride transfer to propene should be preferred instead. Leclerc and Brintzinger [10] thoroughly analyzed the deuterium distribution at the chain end and were able to determine estimates for the different reaction rates. They found that isomerization from **1** to **8** occurs 30–40 times more frequently than chain termination by direct H-transfer. Once the quaternary **8** is formed, further reorientation is 10–15 times faster than chain termination. Chain termination from **8** occurs four to five times more often than from **1**. These observations are in line with our conclusion that **8** has only two possibilities to react: chain termination via H-transfer or, more probably, reorientation via β-H-elimination.

Uncertainties in the calculated energies notwithstanding, the intramolecular stepwise mechanism appears to be only slightly disfavored over intermolecular chain termination reactions like H-transfer or vinylic C–H-activation and should therefore play an important role in the experiment.

Acknowledgements

The authors gratefully acknowledge fruitful discussions with T. Ziegler. J.C.W.L. wants to thank the Fonds der Chemischen Industrie for financial support through a Liebig Stipendium.

References

[1] H.H. Brintzinger, D. Fischer, R. Mülhaupt, B. Rieger, R.M. Waymouth, Angew. Chem. 107 (1995) 1255; Angew. Chem. Int. Ed. Engl. 34 (1995) 1143.
[2] W. Kaminsky, K. Külper, H.H. Brintzinger, F.R.W.P. Wild, Angew. Chem. 97 (1985) 507; Angew. Chem. Int. Ed. Engl. 24 (1985) 507.
[3] J.A. Ewen, J. Am. Chem. Soc. 106 (1984) 6355.
[4] D. Veghini, L.M. Henling, T.J. Burkhardt, J.E. Bercaw, J. Am. Chem. Soc. 121 (1999) 564.
[5] L. Cavallo, G. Guerra, P. Corradini, L. Resconi, R.M. Waymouth, Macromolecules 26 (1993) 260.
[6] L. Cavallo, G. Guerra, M. Vacatello, P. Corradini, Macromolecules 24 (1991) 1784.
[7] P. Corradini, G. Guerra, M. Vacatello, V. Villani, Gazz. Chim. Ital. 118 (1988) 173.
[8] P. Corradini, G. Guerra, Prog. Polym. Sci. 16 (1991) 239.
[9] M.K. Leclerc, H.H. Brintzinger, J. Am. Chem. Soc. 117 (1995) 1651.
[10] M.K. Leclerc, H.H. Brintzinger, J. Am. Chem. Soc. 118 (1996) 9024.
[11] M.H. Prosenc, H.H. Brintzinger, Organometallics 16 (1997) 3889.
[12] T.K. Woo, L. Fan, T. Ziegler, Organometallics 13 (1994) 2252.
[13] T.K. Woo, L. Fan, T. Ziegler, in: G. Fink, R. Mülhaupt, H.H. Brintzinger (Eds.), 40 Years Ziegler-Catalyses, Springer Verlag, Berlin, 1995, p. 291.
[14] H. Weiss, M. Ehrig, R. Ahlrichs, J. Am. Chem. Soc. 116 (1994) 4919.
[15] L. Fan, D. Harrison, L. Deng, T.K. Woo, D. Swerhone, T. Ziegler, Can. J. Chem. 73 (1995) 989.
[16] J.C.W. Lohrenz, T.K. Woo, L. Fan, T. Ziegler, J. Organomet. Chem. 497 (1995) 91.
[17] J.C.W. Lohrenz, T.K. Woo, T. Ziegler, J. Am. Chem. Soc. 117 (1995) 12793.
[18] P. Margl, J.C.W. Lohrenz, T. Ziegler, P.E. Blöchl, J. Am. Chem. Soc. 118 (1996) 4434.
[19] L. Fan, D. Harrison, T.K. Woo, T. Ziegler, Organometallics 14 (1995) 2018.
[20] P. Margl, L. Deng, T. Ziegler, J. Am. Chem. Soc. 120 (1998) 5517.
[21] P. Margl, L. Deng, T. Ziegler, Organometallics 17 (1998) 933.
[22] P. Margl, L. Deng, T. Ziegler, J. Am. Chem. Soc. 121 (1999) 154.
[23] F.U. Axe, J.M. Coffin, J. Phys. Chem. 98 (1994) 2567.
[24] E.J. Baerends, ADF 1.1.3, Vrije Universiteit, Amsterdam, 1995.
[25] W. Ravenek, in: H.J.J.t. Riele, T.J. Dekker, H.A.v.d. Vorst (Eds.), Algorithms and Applications on Vector and Parallel Computers, Elsevier, Amsterdam, 1987.

[26] P.M. Boerrigter, G. teVelde, E.J. Baerends, Int. J. Quantum Chem. 33 (1988) 87.
[27] G. teVele, E.J. Baerends, J. Comput. Phys. 99 (1992) 84.
[28] L. Versluis, T. Ziegler, J. Chem. Phys. 88 (1988) 322.
[29] J.G. Snijders, P. Vernooijs, E.J. Baerends, At. Nucl. Data Tables 26 (1981) 483.
[30] P. Vernooijs, G.J. Snijders, E.J. Baerends, Slater Type Basis Functions for the Whole Periodic System, Free University of Amsterdam, The Netherlands, 1981.
[31] E.J. Baerends, Ph.D. Thesis, Vrije Universiteit, Amsterdam, 1975.
[32] J. Krijn, E.J. Baerends, Fit Functions in the HFS-method, Free University of Amsterdam, The Netherlands, 1984.
[33] S.H. Vosko, L. Wilk, M. Nusair, Can. J. Phys. 58 (1980) 1200.
[34] A.D. Becke, Phys. Rev. A38 (1988) 3098.
[35] (a) J.P. Perdew, Phys. Rev. B 33 (1986) 8822. (b) J.P. Perdew Phys. Rev. B 34 (1986) 7406.
[36] (a) M.J. Frisch, G.W. Trucks, H.B. Schlegel, P.M.W. Gill, B.G. Johnson, M.A. Robb, J.R. Cheeseman, T. Keith, G.A. Petersson, J.A. Montgomery, K. Raghavachari, M.A. Al-Laham, V.G. Zakrzewski, J.V. Ortiz, J.B. Foresman, C.Y. Peng, P.Y. Ayala, W. Chen, M.W. Wong, J.L. Andres, E.S. Replogle, R. Gomperts, R.L. Martin, D.J. Fox, J.S. Binkley, D.J. DeFrees, J. Baker, J.J.P. Stewart, M. Head-Gordon, C. Gonzales, J.A. Pople, Gaussian 94, Pittsburgh PA, 1995.
[37] H. Horn, unpublished; obtained from the Ahlrichs group (http://www.chemie.uni-karlsruhe.de/PC/TheoChem), see also: A. Schäfer, H. Horn, R. Ahlrichs, J. Chem. Phys. 97 (1992) 2571.
[38] S.P. Walch, C.W. Bauschlicher, C.J. Nelin, J. Chem. Phys. 79 (1983) 3600.
[39] W.J. Hehre, R. Ditchfield, J.A. Pople, J. Chem. Phys. 56 (1972) 2257.
[40] P.C. Hariharan, J.A. Pople, Theor. Chim. Acta 28 (1973) 213.
[41] D. Andrae, U. Häussermann, M. Dolg, H. Stoll, H. Preuss, Theor. Chim. Acta 77 (1990) 123.
[42] T.H. Dunning, J. Chem. Phys. 55 (1971) 716.
[43] A.D. Becke, J. Chem. Phys. 98 (1993) 5648.
[44] C. Lee, W. Yang, R.G. Parr, Phys. Rev. B 37 (1988) 785.
[45] see however: F. Bernardi, A. Bottoni, G. Pietro Miscione, Organometallics 17 (1998) 16.
[46] J.C.W. Lohrenz, T. Ziegler, to be published.
[47] V. Busico, R. Cipullo, J. Am. Chem. Soc. 116 (1994) 9329.
[48] V. Busico, R. Cipullo, J. Organomet. Chem. 497 (1995) 113.
[49] V. Busico, Makromol. Chem. Macromol. Symp. 89 (1995) 277.
[50] B. Rieger, X. Mu, D.T. Mallin, M.D. Rausch, J.C.W. Chien, Macromolecules 23 (1990) 3559.
[51] B. Rieger, J.C.W. Chien, Polym. Bull. 21 (1989) 159.
[52] A.E. Reed, L.A. Curtiss, F. Weinhold, Chem. Rev. 88 (1988) 899.
[53] K. Wiberg, Tetrahedron 24 (1968) 1083.
[54] C. Gonzales, H.B. Schlegel, J. Chem. Phys. 90 (1989) 2154.
[55] C. Gonzales, H.B. Schlegel, J. Phys. Chem. 94 (1990) 5523.
[56] (a) V. Busico, R. Cipullo, P. Corradini, Makromol. Chem. Rapid Commun. 13 (1992) 15. (b) V. Busico, R. Cipullo, P. Corradini, Makromol. Chem. Rapid Commun. 13 (1992) 21. (c) V. Busico, R. Cipullo, P. Corradini, Makromol. Chem. Rapid Commun. 14 (1997) 97.
[57] See, for instance, W. Koch, R. Hertwig, in: P.v.R. Schleyer (Ed.), Encyclopedia of Computational Chemistry, Wiley, Chichester, 1998, pp. 689–698.